Cluster-based reduced-order modeling of the transonic wake of a generic space launcher configuration

By S. Loosen†, E. Kaiser‡, B. R. Noack¶, W. Schröder†.

† Institute of Aerodynamics and Chair of Fluid Mechanics
RWTH Aachen University, Wüllnerstraße 5a, 52062 Aachen, Germany

‡ Department of Mechanical Engineering
University of Washington, Seattle, WA 98195, United States

¶ LIMSI-CNRS, UPR 3251, 91405 Orsay cedex, France

The turbulent wake of a generic planar space launcher configuration is numerically investigated at transonic freestream conditions ($M_\infty = 0.8$ and $Re_D = 6 \cdot 10^5$) using a zonal RANS/LES-method. For the understanding of the asymmetrical loads acting on the engine extension of space launchers, the time resolved turbulent wake flow field is analyzed using cluster-based reduced-order modeling (CROM) to distil dominant coherent structures hidden in the multiple spatio-temporal scales of turbulence. First, the time resolved high-dimensional flow snapshots are decomposed into a small number of geometrically close subsets, called clusters which are represented by their center of mass, named centroids. Second, the transitions between the centroids are modeled by a Markov process. Further analysis of the derived model reveals insights into the physical mechanisms in the flow. In the distribution of the streamwise velocity component and the skin-friction coefficient of the resulting centroids, a streamwise elongation and contraction of the separation region and wedge-shaped reattachment regions can be observed. This behavior is similar to the cross-pumping motion previously detected in the same flow configuration by dynamic mode decomposition (DMD). In addition, the extracted CROM modes show a dynamical behavior which is related to the pumping of the recirculation region and cross-flapping of the shear layer.

1. Introduction

The separating and subsequent reattaching flow occurring at the abrupt contour junction between the mainbody and the attached thrust nozzle of classical space launchers exhibits many similarities with the turbulent flow over a backward-facing step (BFS). Due to its simplicity the BFS flow which is characterized by a straight and fixed separation line has become an important test case for separating-reattaching turbulent shear flows. In the last decades the two-dimensional BFS flow has been extensively studied experimentally, e.g., by Bradshaw & Wong [1], Eaton & Johnston [2], Driver et al. [3], and Simpson [4], and numerically, e.g., by Friedrich & Arnal [5], Silveira Neto et al. [6], Le et al. [7], and Lee & Sung [8]. The main flow features of the BFS flow are summarized in Fig. 1. In nearly all of the above mentioned studies, two types of fluctuating motions are found. The lower frequency mode at a Strouhal number of $Sr_h = 0.012 - 0.014$ based on the step height and the freestream velocity reflects an overall increase and decrease of the separation bubble or shear-layer "flapping" as it is commonly called in the literature. As a result of the flapping motion the instantaneous impingement location of the separated shear layer varies by about two step heights around the mean reattachment position. The "flapping" motion was firstly explained by Driver et al. [3] who attributed the shrinking size of the separation bubble to large vortical structures containing more forward momentum than its neighbors escaping the reattachment region without losing too much mass to the recirculation bubble. The higher frequency mode exhibiting a more broadband spectrum with a Strouhal number between $Sr_h = 0.065 - 0.08$ is attributed to a spanwise Kelvin-Helmholtz like vortex formation and shedding at the step corner. According to Driver et al. [3], the energy spectrum of the pressure fluctuations is predominated by the higher frequency shedding of spanwise vortical structures and the low-frequency flapping motion only contributes little to the total energy. More recently, Statnikov et al. [9] and Scharnowski et al. [10] analyzed the three-dimensional wake of a generic planar launcher consisting of a BFS with a long forebody. It was shown that the reattachment position varies over time not only in the streamwise but also in the spanwise direction leading to a formation of wedge-shaped reattachment regions. Using a DMD analysis this variation in the reattachment process can be traced back to a coherent longitudinal cross-pumping motion of the recirculation bubble at $Sr_h = 0.012$ and a cross-flapping motion of the shear layer at $Sr_h = 0.07$.

Besides the presented studies on planar configurations many experimental and numerical investigations on different axisymmetric configurations ranging from axisymmetric backward-facing steps up to scaled real launchers including the solid booster have been conducted, e.g., Deprés et al. [11], Deck & Thorigny [12], Pain et al. [13], Marié et al. [14], Schrijer et al. [15], and Statnikov et al. [16, 17] . Schrijer et al. used proper orthogonal decomposition (POD) to analyze a time series of snapshots of 2D-PIV measurements and detected two dominant wake modes containing the majority of the turbulent kinetic energy. The first low frequency mode captures an oscillating growing and shrinking of the separation zone, most probably being the counterpart of the shear-layer "flapping" detected in the planar BFS flows or to the more recently observed three-dimensional cross-pumping motion by Statnikov et al. [9] in a planar space launcher configuration. The second higher frequency mode describes an undulating motion of the shear layer coinciding with the vortex-shedding of the BFS flow (Le et al. [7]) and the cross-flapping motion of the planar space launcher (Statnikov et al. [9]). Deprés et al. [11] and Deck & Thorigny [12] experimentally and numerically investigated the wake of an axisymmetric launcher configuration. Using two-point correlation analysis on the instantaneous wall pressure signal located at opposite sides in the azimuthal direction on the nozzle, an anti-phase oscillation at a Strouhal number of $Sr_D \approx 0.2$ was detected causing undesired side loads. They assumed that those periodic side loads are generated by helical vortical structures in the wake. Such a helical mode, however, has not been visualized yet. More recently, Statnikov et al. [9] performed a dynamic mode decomposition of the flow around a generic Ariane 5-like configuration to analyze the coherent structures being responsible for the side forces. Three distinct modes at $Sr_D \approx 0.1; 0.2; 0.35$ were detected. The low frequency mode describes a longitudinal cross-pumping motion of the separation region, the second mode is associated with a cross-flapping motion of the shear layer caused by antisymmetric vortex shedding, and the high frequency mode represents a swinging motion of the shear layer.

The above summarized unsteady behavior of separating/reattaching flows and the connected pressure fluctuations and dynamic loads can lead to undesired structural

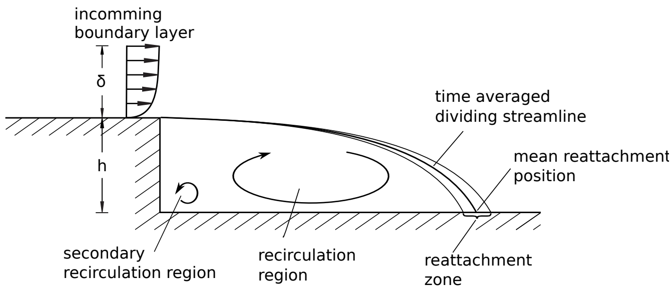

FIGURE 1. Sketch of the topology of a backward-facing step flow

vibrations known as the buffeting phenomenon, if the frequency of the loads excites structural modes of the thrust nozzle. During the high dynamic pressure phase of the flight at a freestream Mach number of $M_\infty = 0.8$, the aerodynamic loads feature the highest amplitudes which can disturb the launchers stability or even result in critical structural damage leading to a complete loss of the launcher under unfavorable circumstances. Because of the highly turbulent character of the wake flow, an accurate prediction of the dynamic loads is still a challenging task. In practice, this leads to increased safety margins and thereby to an overall reduced efficiency of the launcher. For the design of future more efficient and reliable space launcher systems, it is essential to precisely predict these buffet loads and to develop efficient flow control devices to stabilize the wake dynamics and to avoid the buffet phenomenon without penalizing the launcher's total performance. Therefore, a profound understanding and description of the wake flow mechanisms and their interaction is necessary which can be achieved by a reduced order model that describes the intricate wake flow by a reduced number of modes.

An alternative technique to extract spatio-temporal structures and their dynamic interactions is cluster-based reduced-order modeling. CROM is a relatively novel framework originally introduced by Kaiser et al. [18] for the identification of physical mechanisms and transition processes in complex systems like turbulent mixing layers. In particular, it combines cluster analysis and transition matrix models to frame high-dimensional, nonlinear dynamics into a low-dimensional, linear model in the probability space and has strong connections to linear operators of dynamical systems, such as Perron-Frobenius and Koopman operators [19]. As demonstrated below CROM yields spatio-temporal modes associated with particular frequencies and/or decay rates. Moreover, the framework yields a linear model that incorporates nonlinear mechanisms, which is particular useful facilitating estimation, prediction and control of nonlinear systems. In this study, the three-dimensional turbulent wake flow of a planar space launcher at $Ma_\infty = 0.8$ is investigated using CROM to distil the physical mechanisms leading to the periodic undesired dynamic loads on the nozzle structure. In particular, we demonstrate how spatio-temporal modes representing the dominant coherent structures can be extracted from data using CROM. The time resolved flow is computed using a zonal RANS-LES approach.

The paper is organized as follows. In Sec. 2, the investigated geometry and the flow parameters including the zonal RANS/LES method and the computational grids are presented. The CROM framework and the model selection process using information criteria is briefly described in Sec. 3. In Sec. 4, the results of the simulation are presented. First, a short description of the wake flow topology is given. Then, the findings of the

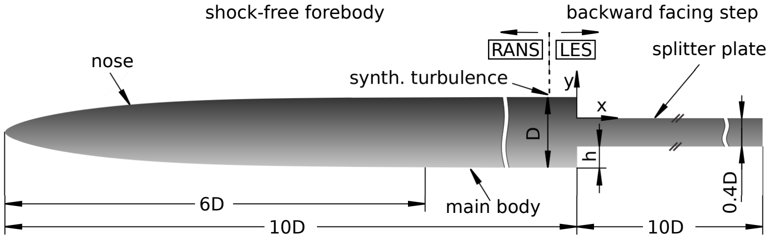

FIGURE 2. Geometry parameters of the investigated generic planar transonic configuration.

cluster analysis applied to the LES data and the identified CROM model and its properties are presented. Finally, conclusions are drawn in Sec. 5.

2. Numerical simulation

In this section, the computational approach, i.e., the investigated geometry and flow parameters, the zonal RANS/LES method, and the computational grid is discucced.

2.1. *Geometry and flow conditions*

The geometry of the investigated generic planar space launcher is given in Fig. 2. The launcher model, which was defined in the framework of the German Collaborative Research Center Transregio 40 [9], is composed of a long shock-free forebody to avoid undesired shock-boundary interaction upstream of the investigated wake flow area and a backward-facing step. The forebody consists of a main body with a reference thickness of D and a length of $4\,D$ and a long nose with a length of 6D. The main body diameter D and the step height $h = 0.3D$ of the BFS are chosen as reference values. The origin of the frame of reference is located in the lower corner of the BFS. The x-axis defines the streamwise direction and the y-axis the wall-normal direction.

Since the dynamic loads feature the highest nominal amplitudes during the transonic stage of the flight trajectory [20], the simulations are performed at a freestream Mach number of $M_\infty = 0.8$. The Reynolds number based on the thickness D of the space launcher is $Re_D = 0.6 \cdot 10^6$

2.2. *Zonal RANS/LES flow solver*

The time resolved computations are performed using a zonal RANS/LES solver which is based on a finite-volume method. The computational domain is split into two zones, see Fig. 3. In the zones where the flow is attached, i.e., the flow around the forebody the RANS equations are solved. The wake flow characterized by the separated shear layer is determined by the LES.

The Navier-Stokes equations of a three-dimensional unsteady compressible fluid are discretized second-order accurate using a mixed centered/upwind advective upstream splitting method (AUSM) scheme for the Euler terms. The non-Euler terms are approximated by a second-order accurate centered scheme. For the temporal integration an explicit 5-stage Runge-Kutta method of second-order accuracy is used. The monotone integrated LES (MILES) method determines the impact of the sub-grid scales. The solution of the RANS equations is based on the same discretization method. To close the time averaged equations the one-equation turbulence model of Fares & Schröder [21] is used. For a comprehensive description of the flow solver see Statnikov et al. [9, 22] .

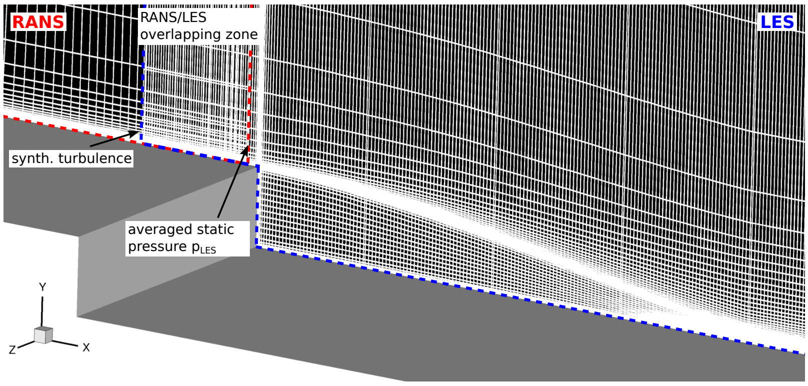

FIGURE 3. Zonal grid topology, every 4th grid point is shown.

2.3. *Computational mesh*

In the zonal approach, the computational domain is divided into a RANS part enclosing the attached flow around the forebody and an LES grid for the wake, as shown in Fig. 3. To reduce the computational costs, the simulation is only performed for the upper half of the flow field. The RANS domain around the forebody extends to approximately 10D in the wall-normal direction and ends at $x/D = -0.05$ just upstream of the trailing edge of the main body located at $x/D = 0$. The LES section extends in the streamwise direction from $x/D = -0.5$ to $x/D = 10$ and in the wall-normal direction, like the RANS mesh from $y/D = 0$ to $y/D = 10$. To ensure a fully developed boundary layer a transition length of approximately three boundary-layer thicknesses is required by the RSTG approach. Since the boundary-layer thickness directly upstream of the base shoulder is $\delta = 0.15D$, the LES inflow plane is positioned at $x/D = -0.5$ to guarantee a fully developed turbulent boundary layer upstream of the BFS geometry.

The characteristic grid resolution in the area within the transition zone in inner wall units $l^+ = u_\tau/\nu$ is $\Delta x^+ = 50$, $\Delta y^+ = 2$, and $\Delta z^+ = 30$ for the LES zone and $\Delta x^+ = 350$, $\Delta y^+ = 1$, and $\Delta z^+ = 1500$ for the RANS domain. The resolution is chosen according to typical mesh requirements in wall-bounded flows outlined by Choi & Moin [23]. In total, 125 million grid points are used for the zonal setup.

3. Methodology

In the following, we will consider a high-dimensional state $\mathbf{u} \in \mathbb{R}^N$ with $N \gg 1$, which may be obtained from experiments or by discretizing a partial differential equation (PDE), that is governed by a nonlinear dynamical system

$$\frac{d}{dt}\mathbf{u} = \mathbf{f}(\mathbf{u}). \tag{3.1}$$

We assume that a collection of high-dimensional velocity field data is available, which is denoted by $\{\mathbf{u}(\mathbf{x}, t_m)\}_{m=1}^{M}$, where $\mathbf{u}(\mathbf{x}, t_m)$ is the m-th realization at time $t_m = m\Delta t$ with constant timestep Δt over a fixed domain Ω with spatial coordinate $\mathbf{x}$.

3.1. *Cluster-based reduced-order modeling (CROM)*

Cluster-based reduced-order modeling was introduced in [18] to discover the underlying low-dimensional dynamics of complex systems in an unsupervised manner, inspired by works in cluster analysis (Burkardt et al. [24]) and transition matrix models (Schneider et al. [25]) in fluid dynamics. CROM is a data-driven, equation-free strategy that frames high-dimensional, nonlinear dynamics into low-dimensional, linear, probabilistic dynamics. First, k-means clustering [26] is employed to partition the data into few groups, called *clusters*, whose members exhibit similar kinematic features. Then, interactions between those clusters are modeled as a Markov process. Further analysis of the model reveals insights into properties of the attractor, e.g., different dynamical regimes and precursors to desirable and undesirable events can be identified. The CROM framework has been recently extended to incorporate control [27] and for the placement of sensors which yield topologically identical models [28].

K-means clustering is a heuristic algorithm that aims to group observations such that the similarity of those belonging to the same group is maximized, while that of those belonging to different groups is minimized. The clusters are represented by their center of mass, called centroids, which yield a low-dimensional kinematic description of the flow data. The data space is partitioned into K centroidal Voronoi cells [29] by minimizing the total cluster variance defined by

$$\{\mathbf{c}_1,\ldots,\mathbf{c}_K\} = \arg\min_{\mathbf{c}'_1,\ldots,\mathbf{c}'_K} \sum_{k=1}^{K} \sum_{\mathbf{u}^m\in\mathcal{C}'_k} ||\mathbf{u}^m - \mathbf{c}'_k||^2_\Omega\,, \tag{3.2}$$

where $\mathbf{u}^m$ denotes the observation, e.g., velocity field, at discrete time t_m and $\mathbf{c}_k$ is the centroid computed as the mean of all observations affiliated with cluster $\mathcal{C}_k$. K-means does not scale well with the dimension of the state, thus data is typically first transformed using, e.g., POD, and k-means is then applied to the temporal POD coefficients, $\mathbf{a}^m = \mathbf{\Psi}^T\mathbf{u}^m\,\forall\, m$. If the data exhibits a low-rank structure, the process can be accelerated further by truncating the basis in $\mathbf{\Psi}$. However, this is not required for the approach and it is advisable not to remove high-order features, which may be important. Similar to modal decompositions such as proper orthogonal decomposition [30] or dynamic mode decomposition [31,32], the centroids are the representative states of the flow. In contrast to DMD modes, which are pure frequency modes, and POD modes, which are resolved by energy content yielding mixtures of frequencies, centroids represent coarse regions in state space exhibiting similar behavior. For strictly periodic flows, for instance, the clustering yields coarse phase bins generalizing phase averaging.

By analysis of the temporal sequence of the observations, the propagator $\mathbf{P}$ of the Markov model can be determined. The transition probabilities between clusters are given by the maximum likelihood estimator (MLE) corresponding to

$$P_{jk} = \frac{\mathrm{card}\{\mathbf{u}^m \in \mathcal{C}_k \text{ and } \mathbf{u}^{m+1}\in\mathcal{C}_j\}}{\mathrm{card}\{\mathbf{u}^m\in\mathcal{C}_k\}} \tag{3.3}$$

where 'card' denotes the cardinality. A coarse-grained probability vector on the state space taking into account uncertainties can be evolved by powers of the propagator,

$$\mathbf{p}_{t+1} = \mathbf{P}\mathbf{p}_t \quad \rightarrow \quad \mathbf{p}_t = \mathbf{P}^t\mathbf{p}_0 \tag{3.4}$$

with $\mathbf{p}_t = [p_1^t,\ldots,p_K^t]^T$ where p_k^t denotes the probability that an observation at time t lies in the cluster $\mathcal{C}_k$. Spectral properties of the transition matrix give insight into multimodal behavior, i.e., regions in state space in which the system stays for a long time before it switches to a different region, and the long-term behavior. There exists a strong connection to the emerging field of linear operators, such as Koopman and its dual, the Perron-Frobenius operator, for the analysis of nonlinear flows. In particular, the resulting

CROM model corresponds to an approximation of the Perron-Frobenius operator [33]. Thus, CROM is aligned with powerful techniques where nonlinear mechanisms are captured in linear frameworks.

3.2. *Model selection via information criteria*

The accuracy and predictive capabilities of the transition model of CROM depend on the length of the available data M, the number of clusters K for the partitioning, and the time step τ of the model. While the limit $K \to M$ yields the most deterministic model, i.e., after one iteration of the model a new cluster is visited with high probability, its transition probabilities have a higher sensitivity to false transitions and the model complexity increases, i.e., it is difficult to analyze with a large number of clusters. In contrast, in the limit $K \to 1$ the model is simple but does not resolve any dynamic process. Here, we employ a model selection approach based on information criteria to select good parameters K and τ. In particular, we employ the Bayesian information criterion (BIC) [34], which is commonly used to identify the optimal order of transition matrix models [35]. The BIC is defined as

$$BIC = -2\ln(L) + k\ln(M) \tag{3.5}$$

where L is the maximum value of likelihood obtained using MLE. The second term penalizes the complexity of the model in terms of the number of parameters k to avoid overfitting. Thus, BIC and similarly the Akaike information criterion are used to compare different models and seek a balance between model fit and complexity.

4. Results

We present cluster-based reduced-order modeling of the wake of a generic space launcher. We first discuss the wake flow topology to obtain an understanding of the principal flow behavior. Then, the best model is selected based on the information criterion and the corresponding state space partitioning and dynamic model is presented. Finally, we extract modes from the model associated with spatio-temporal coherent structures.

4.1. *Wake flow topology*

The wake flow topology of the space launcher is shortly described, since this is important for the overall understanding of the paper. The incoming transonic flow accelerates along the forebody and separates at the sudden geometry change at the tail of the main-body. The turbulent structures of the resulting free-shear layer are visualized in Fig. 4 using Q-contours. The initial small turbulent structures grow in size comparable to the structures observed in planar free-shear layers by Winant & Browand [36], leading to a continuous broadening of the shear layer. After three step heights the initial mainly in the streamwise direction oriented vortices are replaced by three-dimensional structures approaching the lower wall. Further downstream, the shear layer reattaches on the splitter plate approximately between $4 < x/h < 9$ depending on the spanwise position and time. The turbulent wake is characterized by a large number of three-dimensional structures exhibiting various time and length scales that makes a straight forward interpretation of the instantaneous flow field quite complicated. To detect the dominant modes hidden in the multiple spatio-temporal scales of turbulence, we have performed a CROM analysis of the three-dimensional wake flow which is discussed in the following. A more detailed description of the turbulent wake of the investigated planar generic

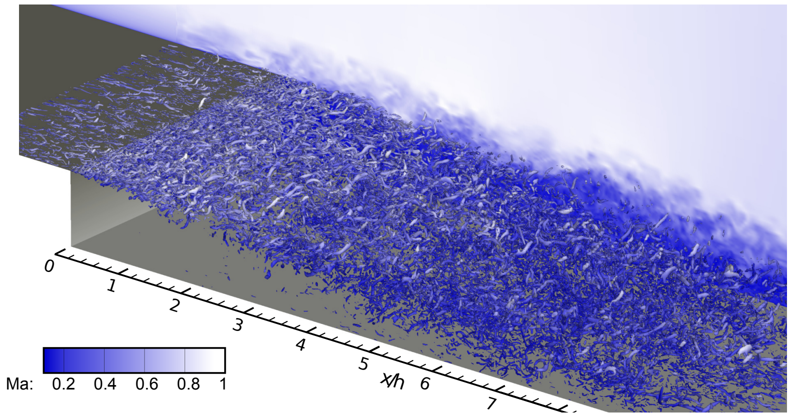

FIGURE 4. Instantaneous wake topology; visualization of the turbulent structures using Q-contours colored by the instantaneous Mach number.

space launcher showing the characteristic spatial and temporal scales of the unsteady wake flow is given in [9].

4.2. *Cluster-based reduced-order modeling*

We demonstrate the selection of a model dependent on the number of clusters K and its time step using the BIC. If one-step transitions between clusters are analyzed, the time step of the model becomes $\tau = 1\Delta t$, where Δt is the time step of the data. However, in order to determine a model with time step $\tau = n\Delta t$, commonly referred to as n-step transition matrix, transition probabilities are determined by examining transitions that occur over $n\Delta t$. For small K, the BIC displays a strong variation with both increasing K and τ (see Fig. 5(a)). In contrast, for large K, BIC is dominated by K and τ has diminishing influence, which is also visible in Fig. 5(b). Smaller values of BIC indicate better models. In particular, we choose the model with K, which is a local minimum and is large enough to resolve the main transition process, and $\tau = 48\Delta t$, which yields the most deterministic model.

The data is partitioned into K cluster and k-means is repeated 10 times to select the most parsimonious model. The Voronoi diagram (see Fig. 6) is obtained using multi-dimensional scaling to compute a two-dimensional feature space that approximately preserves the mutual distances between centroids in the high-dimensional data space. We can make several observations from Fig. 6: (1) The time series of the data is proba-

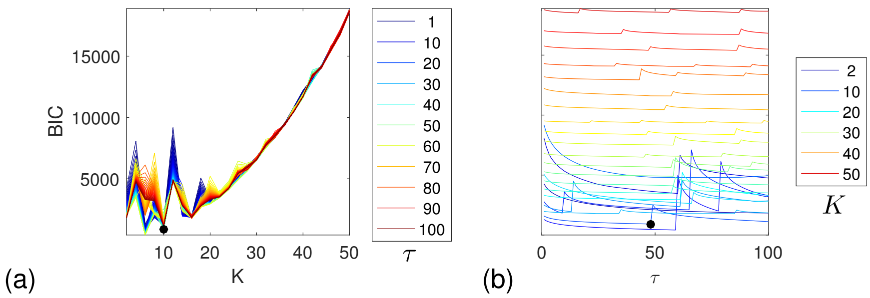

FIGURE 5. Model selection using BIC for increasing (a) number of clusters K, and (b) time step τ. Curves are color-coded for either varying τ or K. Black circle represent selected model.

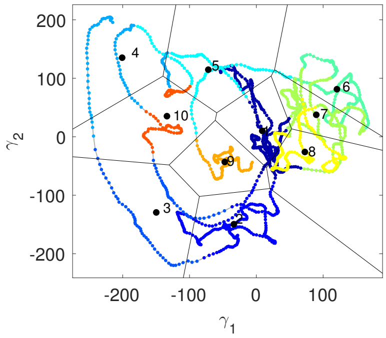

FIGURE 6. Partitioning of the state space using clustering visualized as Voronoi diagram. Each point represents a snapshot at an instance in time color-coded by cluster affiliation.

bly not converged on the attractor or sufficiently long enough, which is corroborated by the fact that the trajectory starts initially in cluster 9, but never visits this cluster again. (2) The time series also may not be sufficient for a statistical analysis. Many clusters are only passed through a few times, such as clusters 3,4,9, and 10. These observations may pose additional challenges in the modeling process.

The velocity centroids computed on the centerline are displayed in Fig. 7. In particular, a streamwise elongation and contraction of the separation region becomes visible in the streamwise velocity component, e.g., when comparing cluster 4 and 10. This is related to the flapping behavior of the recirculation area. Also a vertical expansion and contraction of the extension of the separation region can be observed, e.g., when comparing clusters 9 and 10.

We also show the centroids based on the skin-friction coefficient in Fig. 8. In this

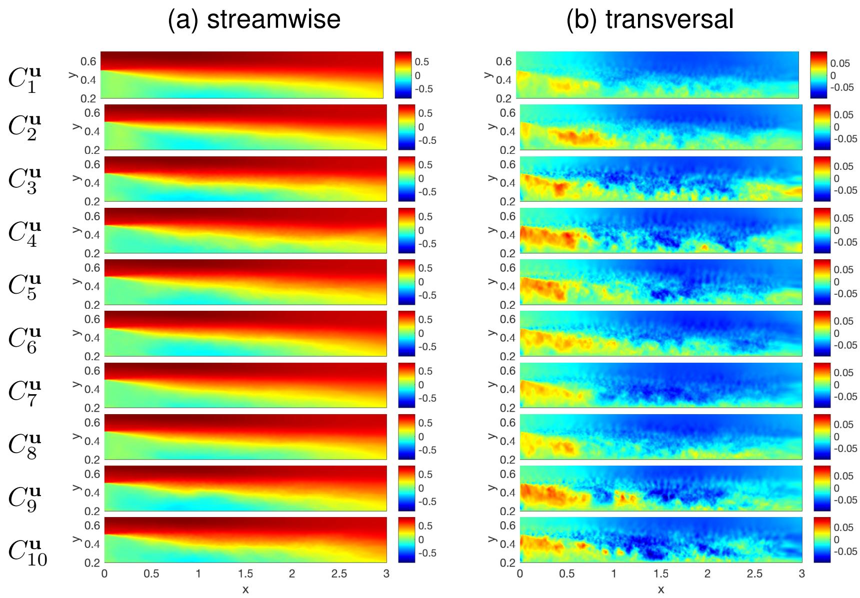

FIGURE 7. Cluster centroids for the (a) streamwise and (b) transversal velocity component along the centerline with $z = const.$

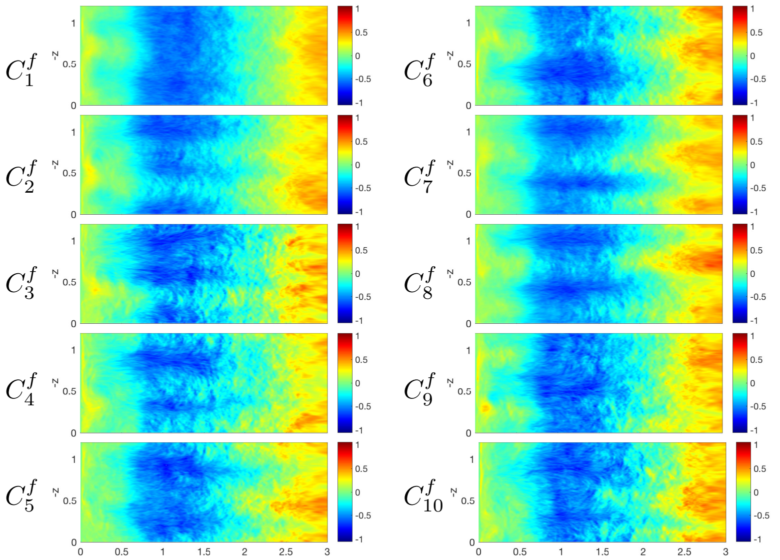

FIGURE 8. Cluster centroids of the skin-friction coefficient at the wall.

configuration wedge-shaped reattachment regions have been observed, which is also captured by the skin-friction centroids. The spanwise variation of these wedges over different centroids indicates their unsteady behavior. Furthermore, in contrast to all other clusters, centroid 1 exhibits a reattachment point which is nearly constant in spanwise direction.

A flow exhibiting dominant, recurring patterns suggests that the essential dynamics evolve on a low-dimensional attractor, which facilitates the development of reduced-order models. The transonic wake of the space launcher is a highly turbulent flow displaying a complex interaction between several low- and high-frequency phenomena, such as the cross-pumping motion of the recirculation bubble and the cross-flapping motion of the shear layer. Thus, extracting low-dimensional patterns and their dynamical interaction is particularly challenging.

The model that provided the best balance between accuracy and complexity and se-

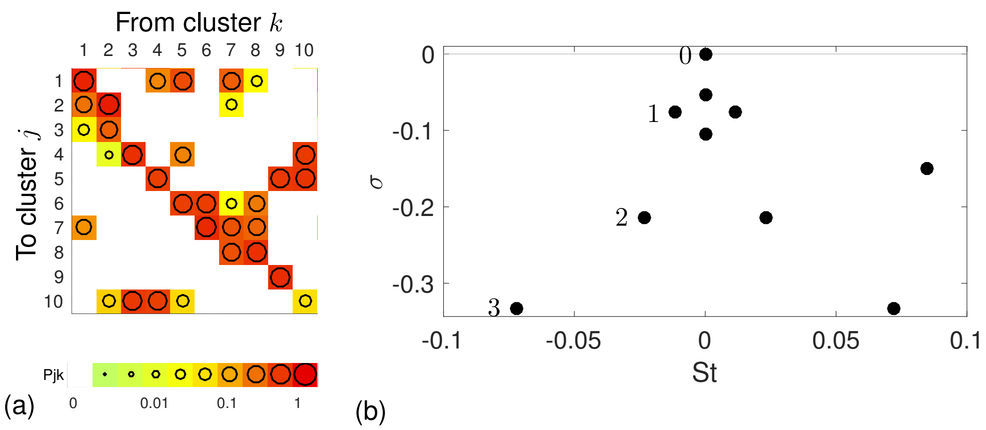

FIGURE 9. Dynamic model for the transonic wake flow: (a) transition probability matrix of CROM and (b) corresponding continuous-time spectrum. Eigenvalues are numbered for later reference.

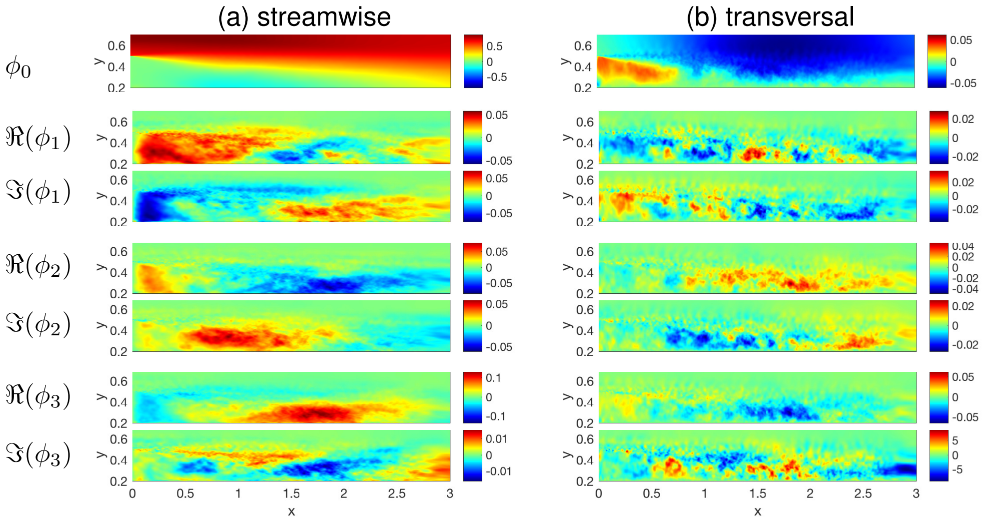

FIGURE 10. First three CROM modes for the (a) streamwise and (b) transversal velocity fluctuation component along the centerline with $z = const.$

lected using BIC, is presented in Fig. 9 together with its continuous-time spectrum. In most clusters, the probability that the trajectory resides in this cluster over the timestep of the model is zero or very small. The model is still very parsimonious with few transitions between clusters with comparably large probabilities, which suggest that this model could be predictive.

From the eigenvectors of the transition probability matrix we can extract spatio-temporal modes, which can be oscillatory, show no oscillations, and/or have a decay rate. Similarly as DMD modes, oscillatory CROM modes come in pairs and the mode with zero growth/decay rate and frequency (Mode 0) represents the mean flow (compare Fig. 10). Higher-order modes typically represent higher frequencies and wavenumbers. Particularly, Mode 2 seems to capture the expansion and contraction of the recirculation area, while mode 3 seems to be associated with the cross-flapping motion of the shear layer.

In Fig. 11, the first two modes are represented for the skin-friction coefficient and the pressure. Interestingly, the first mode in the skin-friction coefficient captures the dynam-

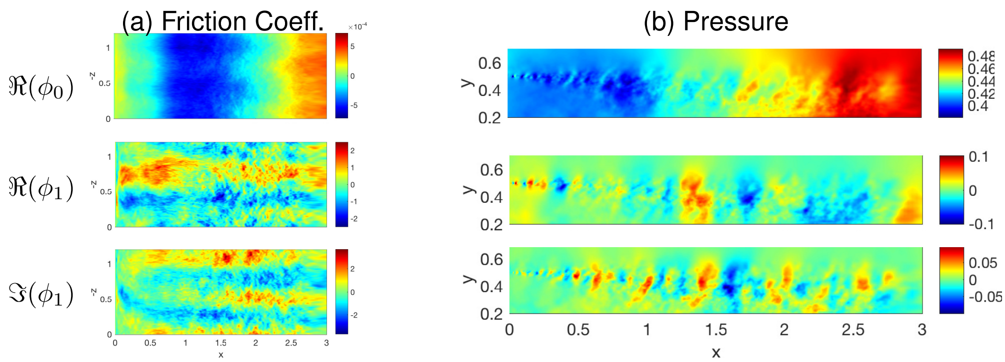

FIGURE 11. First two CROM modes for the (a) fluctuation of the skin-friction coefficient, and (b) the pressure fluctuation along the centerline with $z = const.$

ical behavior of the wedge-like structures. The first mode of the pressure is associated with the shedding of typical shear layer structures. While the velocity modes seem to contain mixed frequency content, the modes of the skin-friction coefficient are much cleaner. The reason lies in the low resolution of the dynamical behavior due to using only $K = 10$ clusters, which seems to affect the velocity much stronger.

5. Summary and conclusions

We presented the cluster-based reduced-order modeling of the transonic wake of a space launcher. An information-based model selection was employed to select the model that provides the best balance between accuracy and complexity. The analysis of the model yields several observations: (1) Certain clusters are associated with the pumping of the recirculation area. (2) CROM modes associated with the dynamical behavior are related to the pumping of the recirculation area and cross-flapping of the shear layer. A further analysis of the forces acting on the nozzle associated with each cluster could provide valuable insight [37]. Moreover, there exists a strong connection between CROM and DMD and the analysis suggests that CROM modes may converge to DMD modes in the limit $K \to M$. If so, CROM could potentially be useful as a mode-filtering approach to select the dynamically most important modes. As CROM is based on the clustering of the state space into few clusters, it naturally filters out subscale structures.

Acknowledgments

Financial support has been provided by the German Research Foundation (Deutsche Forschungsgemeinschaft – DFG) in the framework of the Sonderforschungsbereich Transregio 40. Computational resources have been provided by the High Performance Computing Center Stuttgart (HLRS). EK gratefully acknowledges funding by the eScience Institute, the G. & B. Moore, A. P. Sloan, and the Washington Research Foundations. We thank Steven Brunton for valuable stimulating discussions.

References

[1] BRADSHAW, P. AND WONG, F. (1972). The reattachment and relaxation of a turbulent shear layer. *J. Fluid Mech.*, **52**(1), 113–135.

[2] EATON, J.K. AND JOHNSTON, J.P. (1981). A review of research on subsonic turbulent flow reattachment. *AIAA J.*, **19**(9), 1093–1100.

[3] DRIVER, D.M., SEEGMILLER, H.L. AND MARVIN, J.G. (1987). Time-dependent behavior of a reattaching shear layer. *AIAA J.*, **25**(7), 914–919.

[4] SIMPSON, R.L. (1989). Turbulent boundary-layer separation. *Ann. Rev. Fluid Mech.*, **21**, 205–2034.

[5] FRIEDRICH, R. AND ARNAL, M. (1990). Analysing turbulent backward-facing step flow with the low-pass-filtered Navier-Stokes Equations. *Journal of Wind Engineering and Industrial Aerodynamics*, **35**, 101–128.

[6] SILVERIA NETO, A., GRAND, D., METAIS, O. AND LESIEUR, M. (1993). A numerical investigation of the coherent vortices in turbulence behind a backward-facing step. *J. Fluid Mech.*, **256**, 1–25.

[7] LE, H., MOIN, P. AND KIM, J. (1997). Direct numerical simulation of turbulent flow over a backward-facing step. *J. Fluid Mech.*, **330**, 349–374.

[8] LEE, I. AND SUNG, H.J. (2001). Characteristics of wall pressure fluctuations in separated and reattaching flows over a backward-facing step: Part I. Time-mean statistics and cross-spectral analyses. *Experiments in Fluids*, **30**, 262–272.

[9] STATNIKOV, V., BOLGAR, I., SCHARNOWSKI, S., MEINKE, M., KÄHLER, C.J. AND SCHRÖDER, W. (2016). Analysis of characteristic wake flow modes on a generic transonic backward-facing step configuration. *Europ. J. Mech. B/Fluids*, **59**, 124–134.

[10] SCHARNOWSKI, S., BOLGAR, I. AND KÄHLER, C.J. (2017). Characterization of turbulent structures in a transonic backward-facing step flow. *Flow, Turbulence and Combustion*, **98**(4), 947–967.

[11] DEPRÉS, D., REIJASSE, P. AND DUSSAUGE, J.P. (2004). Analysis of unsteadiness in afterbody transonic flows. *AIAA J.*, **42**(12), 2541–2550.

[12] DECK, S. AND THORIGNY, P. (2007). Unsteadiness of an axisymmetric separating-reattaching flow: Numerical investigation. *Physics of Fluids*, **19**(065103).

[13] R. PAIN, P. E. WEISS, S.D. (2014). Zonal detached eddy simulation of the flow around a simplified launcher afterbody. *AIAA J.*, **52**(9).

[14] MARIE, S., DRUAULT, P., LAMBARE, H. AND SCHRIJER, F. (2013). Experimental analysis of the pressure-velocity correlations of external unsteady flow over rocket launchers. *Aerospace Science and Technology*, **30**, 83–93.

[15] SCHRIJER, F., SCIACCHITANO, A. AND SCARANO, F. (2014). Spatio-temporal and modal analysis of unsteady fluctuations in a high-subsonic base flow. *Physics of Fluids*, **26**(086101).

[16] STATNIKOV, V., MEINKE, M. AND SCHRÖDER, W. (2016). Analysis of spatio-temporal wake modes of space launchers at transonic flow. *AIAA Paper*, **2016-1116**.

[17] STATNIKOV, V., MEINKE, M. AND SCHRÖDER, W. (2017). Reduced-order analysis of buffet flow of space launchers. *J. Fluid Mech.*, **815**, 1–25.

[18] KAISER, E., NOACK, B.R., CORDIER, L., SPOHN, A., SEGOND, M., ABEL, M., DAVILLER, G., ÖSTH, J., KRAJNOVIĆ, S. AND NIVEN, R.K. (2014). Cluster-based reduced-order modelling of a mixing layer. *J. Fluid Mech.*, **754**, 365–414.

[19] LASOTA, A. AND MACKEY, M.C. (1994). *Chaos, Fractals, and Noise*. 2nd edn. Springer New York.

[20] DAVID, S. AND RADULOVIC, S. (2005). Prediction of buffet loads on the Ariane 5 afterbody. *6th International Symposium on Launcher Technologies, Munich, Germany, 8-11 November*.

[21] FARES, E. AND SCHRÖDER, W. (2004). A general one-equation turbulence model for free shear and wall-bounded flows. *Flow Turbul. Combust.*, **73**, 187–215.

[22] STATNIKOV, V., SAYADI, T., MEINKE, M., SCHMID, P. AND SCHRÖDER, W. (2015). Analysis of pressure perturbation sources on a generic space launcher after-body in supersonic flow using zonal turbulence modeling and dynamic mode decomposition. *Physics of Fluids*, **27**(016103).

[23] CHOI, H. AND MOIN, P. (2012). Grid-point requirements for large eddy simulation: Champan's estimates revisited. *Physics of Fluids*, **24**(011702).

[24] BURKARDT, J., GUNZBURGER, M. AND LEE, H. (2006). Pod and cvt-based reduced-order modeling of navier-stokes flows. *Comput. Meth. Appl. Mech. Eng.*, **196**, 337–355.

[25] SCHNEIDERS, T.M., ECKARD, B. AND VOLLMER, J. (2007). Statistical analysis of coherent structures in transitional pipe flow. *Phys. Rev.*, **75**(066313).

[26] BISHOP, C.M. (2007). *Pattern Recognition and Machine Learning*. Springer.

[27] KAISER, E., NOACK, B.R., SPOHN, A., CATTAFESTA, L.N. AND MORZYŃSKI, M. (2017). Cluster-based control of a separating flow over a smoothly contoured ramp. *Theoret. and Comp. Fluid Dyn.*, 1–15.

[28] KAISER, E., MORZYŃSKI, M., DAVILLER, G., KUTZ, J.N., BRUNTON, B.W. AND BRUNTON, S.B. (2016). Sparsity enabled cluster reduced-order models for control. *arXiv:1701.00038*.

[29] DU, Q., FABER, V. AND GUNZBURGER, M. (1999). Centroidal voronoi tessellations: applications and algorithms. *SIAM Rev.*, **41**, 637–676.

[30] HOLMES, P., LUMLEY, J.L., BERKOOZ, G. AND ROWLEY, C.W. (2012). *Turbulence, Coherent Structures, Dynamical Systems and Symmetry*. 2nd paperback edn. Cambridge University Press, Cambridge.

[31] SCHMID, P. (2010). Dynamic mode decomposition of numerical and experimental data. *J. Fluid Mech.*, **65**(6), 5–28.

[32] ROWLEY, C.W., MEZIĆ, I., BAGHERI, S., SCHLATTER, P. AND HENNINGSON, D.S. (2009). Spectral analysis of nonlinear flows. *Journal of Fluid Mechanics*, **641**, 115–127.

[33] BOLLT, E.M. AND SANTITISSADEEKORN, N. (2013). *Applied and Computational Measurable Dynamics*. SIAM.

[34] SCHWARZ, G. (1978). Estimating the dimension of a model. *Ann. Statist.*, **6**(2), 461–464.

[35] KATZ, R.W. (1981). On some criteria for estimating the order of a markov chain. *Technometrics*, **23**(3), 243–249.

[36] WINANT, C.D. AND BROWAND, F.K. (1974). Vortex pairing: The mechanism of turbulent mixing-layer growth at moderate reynolds number. *J. Fluid Mech.*, **63**(2), 237–255.

[37] ÖSTH, J., KAISER, E., KRAJNOVIĆ, S. AND NOACK, B.R. (2015). Cluster-based reduced-order modelling of the flow in the wake of a high-speed train. *J. Wind Eng. Ind. Aerodyn.*, **145**, 327–338.